Direct Simulation Monte Carlo Study of Neutral Temperature, Density, and Pressure in an Inductively Coupled Plasma

Masashi Shimada, Robert Cattolica and George R. Tynan

Department of Mechanical and Aerospace Engineering, Center for Energy Research, University of California, San Diego, Mail code 0417, EBU-II, 9500 Gilman Dr., La Jolla, CA 92093 USA

Abstract. A hybrid type direct simulation Monte Carlo (DSMC) method was applied to a one-dimensional electrostatic plasma in Argon/Nitrogen mixtures to simulate neutral and ion transport in a radial symmetric inductively coupled plasma. The ambi-polar electrostatic field obtained from the measured plasma density profile was imposed in the simulation. Electrons were treated as background particles with measured electron density and temperature profiles. Electron-ion Coulomb collisions, electron-neutral elastic collisions, ion-neutral elastic collisions, ion-nuetral charge exchange, neutral-neutral elastic collisions, and dissociation were included in the simulation. The inductively coupled plasma ($Ar/5\%N_2$) that was simulated was characterized by the following properties: $p_{fill} = 10$ [mTorr], $T_e \sim 2.5$ [eV], $n_e \sim 6 \cdot 10^{17}$ [m^{-3}], $K_n^{iN} \sim \lambda_{iN}/R \sim 0.05$, $K_n^{NN} \sim \lambda_{NN}/R \sim 10^{-3}$ R=0.18 [m]. Neutral gas depletion observed in both the experiment and simulation is in excellent agreement and indicates that gas heating and the required pressure balance is responsible. The gas heating is mainly due to ion-neutral collisions with the ions accelerated by the ambi-polar electric field and neutral collisions with Frank-Condon dissociated atoms. In the high density plasma source ($T_e \sim 2 \sim 5$[eV], $n_e \sim 1 \sim 10 \cdot 10^{17}$ [m^{-3}]), the plasma pressure becomes comparable to neutral pressure. Total pressure (neutral pressure and plasma pressure) is conserved before and after the discharge. Therefore the neutral pressure is reduced due the balance of total pressure with plasma pressure (mainly electron pressure). No effects of plasma pumping was observed in either the experiment or simulation.

Keywords: DSMC, neutral depletion, gas heating
PACS: RGD25 paper Shimada

INTRODUCTION

In plasma etching with an inductively coupled plasma (ICP), neutrals are often assumed to be at room temperature and at constant density, but both temperature and density variation of neutrals have been observed and simulated in low temperature plasma. Variation in the neutral radical density profile can influence processing uniformity; however there have been few systematic studies of the mechanism which leads to non-uniform neutral distribution in processing plasmas.

Hori [1] and Lee [2] measured neutral density profile and concluded that neutral depletion occurs due to neutral gas heating under the assumption of uniform pressure and ideal gas law. Meanwhile Tynan [3, 4] and Yun [5] measured neutral pressure profile and concluded that that neutral depletion occurs due to plasma pumping under the assumption of isothermal neutral and ideal gas law. Theoretical study of Fruchtman [6] showed that the neutral depletion occurred due to the neutral and plasma pressure balance. The author observed that the neutral gas depletion occurred mainly due to the neutral gas heating. There exists at least three mechanisms (plasma pumping, gas heating and pressure balance) to explain the neutral gas depletion. The central theme of this research is to develop a numerical tool to understand the leading mechanism of the neutral gas depletion.

The direct simulation Monte Carlo (DSMC) method was chosen for this research. Since the ionization fraction in this high density plasma is about one percent or less, the majority of species are neutrals. The Knudsen number of neutrals in the high density plasma is $K_n^{iN} \sim \lambda_{iN}/R \sim 0.05$, $K_n^{NN} \sim \lambda_{NN}/R \sim 10^{-3}$, the condition of typical plasma processing. Therefore, the kinetic Monte Carlo treatment of neutrals is required in such a rarefied system.

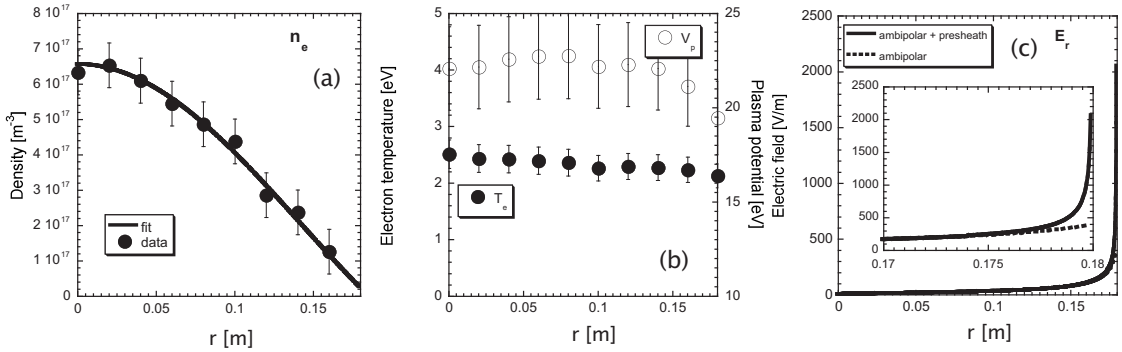

FIGURE 1. (a)Measured radial electron density profile (solid circles) and fit to electron density profile (solid line) with zeroth order Bessel's function (b) Measured radial electron temerature (solid circles) and plasma potential (open circles) profile in $Ar/5\%N_2$ mixture, $p_{fill} = 10$mTorr and $P_{RF} = 2000$W (c) Ambipolar electrostatic field profile calcuated from fit of electron density profile, and pre-sheath electrostatic field within one mean free path from wall.

SIMULATION

General consideration

Neutral and ion transport phenomena were simulated by a hybrid type direct simulation Monte Carlo (DSMC) method for a one-dimensional (1D) electrostatic plasma [7, 8, 9, 10] in Ar/N_2 mixtures. Only ions are affected by this electrostatic field since ion motion is mobility dominated and electron motion is determined by the Boltzmann equilibrium. Electrons were treated as background particles with measured electron density profile and electron temperature profile as shown in fig. 1. Electron-ion Coulomb collision, ion-ion Coulomb collision, electron-neutral elastic collision, ion-neutral elastic collision, ion-neutral charge exchange, neutral-neutral elastic collision and dissociation were considered in the simulation.

The simulation length R is 0.18 [m], which is the radius of the ICP chamber. The cell size Δx and the time step Δt were set to be $\Delta x \sim \frac{\lambda_{mfp}}{5}$ and $\Delta t \sim \frac{\tau}{5} \sim \frac{\Delta x}{5 \cdot V_{th}}$, where λ_{mfp} is the mean free path of a particle, τ is the mean time to travel one cell width, and v_{th} is the thermal velocity. The mean free math λ_{mfp} of a neutral and an ion is about $0.5 \sim 1$cm for the condition of the experiment (Ar plasma: $p_{fill} = 10$ [mTorr], $T_e \sim 3$ [eV], $n_e \sim 5 \cdot 10^{17}$ [m_{-3}], $K_n^{iN} \sim \lambda_{iN}/R \sim 0.05$, $K_n^{NN} \sim \lambda_{NN}/R \sim 10^{-3}$). Therefore, the simulation length R was divided into 100 cells with the cell size $\Delta x = 1.8$[mm], and the time step Δt was chosen to be $\Delta t \sim 5 \cdot 10^{-7}$ [s]. The simulation provides the radial distribution of gas property in a one-dimentional cylindrical geometry. The sheath width is smaller than the cell width, therefore the sheath is neglected in this simulation.

Electrostatic field

Since electrons were treated as the background particles in this simulation, both electric and magnetic fields can not be obtained self-consistently. The ambi-polar electrostatic field can be obtained from the plasma density profile under the assumption of isothermal plasma and non-equilibrium plasma $T_e \gg T_i$ [11, 12]. The plasma density profile was measured and fit to the zeroth order Bessel's function to obtain the ambi-polar electrostatic field as shown in fig. 1 (a). The ambi-polar electrostatic field obtained from measured plasma density profile was used in the simulation, and the pre-sheath electrostatic field was introduced within one mean free path length from wall in order to satisfy the Bohm sheath criterion [13, 14]. Ions follow the electrostatic field and gain energy. The ambi-polar electrostatic field was the order of 10 $[\frac{V}{m}]$, but the calculated pre-sheath electrostatic field became the order of $10^3[\frac{V}{m}]$ as shown in fig. 1 (c).

Initial condition/Boundary condition

About 20000 simulation particles were introduced in this simulation, and the majority of simulation particles were set to be neutral particles depending on the ionization fraction. The weighting factor was used to treat small number of species (ex. ions). The measured plasma density profile was used as the initial radial ion density profile, whereas initial neutral density profile was uniform. Both neutral and ion temperature were initially set at the room temperature ($T_n(t=0,x) \sim T_i(t=0,x) \sim 300$ [K]), and the initial velocities ($v_x^i(t=0), v_y^i(t=0), v_z^i(t=0)$) were generated according to the Maxwellian distribution at the room temperature.

The inner boundary at x=0 [m] was treated as specular reflection to simulate a plane of symmetry. The outer boundary at x=R=0.18 [m] was treated as diffusive reflection. The wall temperature was set to $T_{wall} \sim 350$ [K], velocities off the wall were generated according to the Maxwellian distribution at $T_{wall} \sim 350$ [K]. All the ions that hit the wall were reflected as neutrals, which simulated the surface recombination. The ions that hit the wall with probability of α (the thermal accommodation coefficient) were reflected as neutrals with velocities off the wall generated according to a Maxwellian distribution with $T_{wall} \sim 350$ [K] and remaining ions $(1-\alpha)$ were specular reflected. In order to keep the plasma density constant in the simulation, the same number of neutrals were randomly ionized to become ions in the bulk, which corresponds to volumetric ionization. With the final position of the ion before hitting the wall, the electrostatic field and wall potential, the radial velocity of the ion at the wall can be calculated.

Mass flow rate/Pumping

In the experiment, there is a mass flow inlet as the particle source and there is also mechanical pumping as the particle sink. The particle source is set by the mass flow rate (volumetric flow rate) of a mass flow controller, whereas the particle sink is controlled by a throttle valve keeping the pumping speed constant. While the input volumetric flow rate remains constant, the output volumetric flow rate changes with the pressure of the chamber. When the plasma discharge is turned on, the neutral pressure initially increases as the neutral gas temperature rises. Therefore, the output volumetric flow rate increases and pumps more molecules, then the neutral pressure decreases to the fill pressure. To simulate this mechanism a number of particles at the wall are removed and the same number of particle are introduced randomly in position and with velocity calculated according to the Maxwellian distribution at room temperature $T_{wall} \sim 300$ [K]. When the neutral pressure at the wall increases above the fill pressure with the discharge on, the number of particles pumped away increases keeping the number of particles introduced constant and keeping the neutral pressure at the wall constant [15].

Collisionless motion

The equation of motion for each simulation particle was calculated in each time step Δt [7],

$$\mathbf{v}_i(t+\Delta t) = \mathbf{v}_i(t) + \mathbf{a}(x)\Delta t \tag{1}$$

$$\mathbf{x}_i(t+\Delta t) = \mathbf{x}_i(t) + \mathbf{v}_i(t)\Delta t \tag{2}$$

where $\mathbf{x}_i(t)$ and $\mathbf{v}_i(t)$ are the position and velocity of simulation particle i at time t. The acceleration term $\mathbf{a}(x)$ is zero for neutral and becomes $\mathbf{a}(x) = \frac{e\mathbf{E}(x)}{M}$ for ion, where e is the charge, M is the ion mass, and $\mathbf{E}(x)$ is the electrostatic field at the particle position x. Bluk electrostatic field due to ambipolar diffusion ($T_e >> T_i$) was calculated by the measured plasma density profile. The measured electron density was fit with the zeroth order Bessel's function.

$$n_e(x) = J_0(\frac{\chi x}{R}) \tag{3}$$

where $\chi \sim 2.405$, $J_0(\frac{\chi x}{R})$ are the zeroth order Bessel's function.

$$E_{ambipolar}(x) = -\frac{T_e}{e}\frac{\nabla n_e}{n_e} \tag{4}$$

The electrostatic field used in the simulation is shown in fig. 3. The change in $\mathbf{x}_i$ and $\mathbf{v}_i$ due to the above equation of motion are considered as the collisionless motion.

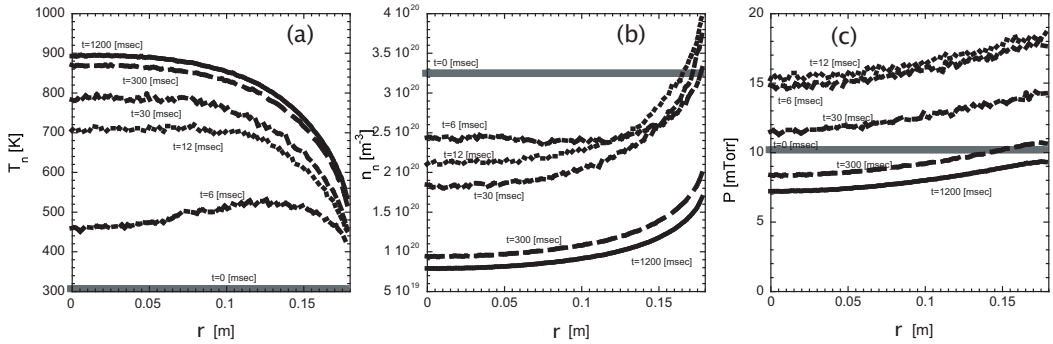

FIGURE 2. Simulation convergence to the steady state (a): Neutral temperature profile, (b): Neutral density profile, (c): Neutral pressure profile, t=0,6,12,30,300,1200 [msec]

Collisions

Electron-ion Coulomb collision, ion-ion Coulomb collision, electron-neutral elastic collision, ion-neutral elastic collision, ion-neutral charge exchange, neutral-neutral elastic collision, and dissociation were considered in the simulation. Electrons were treated as background particles with measured electron density profile and electron temperature profile. Electron-electron Coulomb collisions and inelastic collisions of neutrals with electrons are neglected in the simulation. Also all the collisions with meta stable atoms were neglected.

All collision algorithms used in this simulation are described in detail by Bird [7] and Nanbu [9], and collisions are taken place in each cell. In general, the collision probability is calculated for each collision pair with its relative velocity. A rejection/acceptance method using a random number was used to decide whether the collision actually occurs or not. After each collision, the post-collision velocities were calculated and the pre-collision velocities were replaced by the post-collision velocities.

For the short-range collision beweeen the same species (N-N), the Variable Hard Sphere (VHS) model was used [7]. VHS model is a very efficient way to treat a collision with the differential cross section σ for an inverse-power-potential. The differential cross section is energy dependent, while the scattering angle is not energy dependent.

For the short-range collision between different species (i-N, e-N), the Hard Sphere (HS) model was used [9]. The HS model is a simpler version of the VHS model, which treats collisions as two hard spheres. The differential cross section is not energy dependent. While the scattering angle is not energy dependent for i-N collision, the scattering angle is energy dependent for e-N collision.

For the long-range Coulomb collision (e-i, i-i), Nanbu's method of treating cumulative short-angle collision as one large-angle collision was used [9]. Unlike other collision algorithm, this method does not use the collision probability. The time step Δt plays a role in determining the scattering angle χ. Coulomb collisions can be calculated very efficiently since this method treats many short-angle collisions as one large-angle collision.

Ionization/Surface recombination

In the discharge plasma, the electron temperature and density can be obtained from the particle balance equation and power balance equation respectively [11]. In this simulation the electron temperature and density were set as input parameters, but the particle balance between the volumetric ionization and surface recombination have to be satisfied. Therefore, the volumetric ionization rate ($R_{vol,iz} = n_e n_n < \sigma v >^{iz} V$) was set equal to the surface recombination rate at the wall ($R_{sur,rec} = n_s u_{Bohm} A$). Ions incident upon the wall become neutrals with the velocities according to the Maxwellian distribution with wall temperature $T_{wall} \sim 350$ [K]. Neutrals were ionized randomly in the bulk and then become ions with the same velocities.

Gas Mixture/Dissociation

In previous research on the ICP [16, 17] the spatial profiles of neutral gas temperature, pressure, and density were obtained in $Ar/5\%N_2$ mixture, $p_{fill} = 10$mTorr and $P_{RF} = 2000$W. Even for a few percent ionization fraction significant neutral heating by the dissociated Frank-Condon atom (N atom) is expected. Therefore, the gas mixture and dissociation have to be included in the simulation to compare with previously measured experimental results. The dissociation atom is introduced with the Frank-Condon energy of $\Delta E_{FC} \sim 4$ [eV] at a fixed rate since the electron impact dissociation rate $R_{diss} = n_e n_{N_2} < \sigma v >_{diss}$ of Nitrogen can be calculated with the given electron temperature and density [18, 19].

INITIAL SIMULATION RESULTS

Simulation Convergence

In fig. 2, the simulation convergence to the steady state (t= 6, 12, 30, 300, 1200 [msec]) was shown for neutral temperature, pressure, and density profiles. Fig. 2 (a) shows that neutrals were initially heated close to the wall via elastic/charge exchange collision with ions which were accelerated by the ambipolar electric field. Then heat is diffused toward the center of plasma. Fig. 2 (b) shows that neutral density was decreased due to the neutral temperature increase. Fig. 2 (c) shows that neutral pressure was initially increased and then was decreased due to the wall pumping. The gas heating process is faster than the pumping process, therefore the neutral pressure is initially increased due to the gas heating and then was decreased due to the wall pumping. The total number of neutral particles was significantly reduced by the wall pumping to keep the neutral pressure at the wall at the fill pressure. The neutral pressure convergence was the slowest process. When the neutral pressure at the wall equals the fill pressure, both neutral temperature and density reach the steady state.

Comparison of Numerical and Experimental Results

Fig. 3 shows the comparison of numerical and experimental results for neutral temperature, neutral pressure and neutral density. The spatial variation of neutral gas temperature, pressure, and density were measured at the condition $Ar/5\%N_2$ mixture $p_{fill} = 10$mTorr and $P_{RF} = 2000$W in the inductively coupled plasma (ICP) [16, 17]. The plasma source consists of a 100-mm-diameter Pyrex belljar surrounded by a double loop antenna that is driven at 13.56 MHz. The rf power is coupled to the antenna via a feed back controlled matching network capable of driving the antenna over a wide range of process gases and rf powers. This belljar and plate assembly are located at the top of 350-mm-diameter and 400 mm high anodized aluminum reaction chamber. The following input parameters were used in the simulation $T_e \sim 2.5$ [eV], $n_e \sim 6 \cdot 10^{11}$ [cm^{-3}], $\alpha \sim$ 0.8 for the condition $Ar/5\%N_2$ plasma: $p_{fill} = 10$ [mTorr].

Fig. 3 (a) plots the simulated neutral temperature and ion temperature profiles along with the measured neutral temperature profile. The rotational temperature was measured from second positive band of Nitrogen molecule (v',v")=(0,2) at 380 nm. Ion temperature at the center of plasma is the same as that of neutral $T_i(x = 0) \sim T_n(x = 0)$, and then ion temperature increases toward the wall due to the acceleration via the ambi-polar electric field and the collision with neutrals. The ion temperature reaches $T_i(x = R) \sim 6000$[K].

Fig. 3 (b) shows the simulated neutral pressure, total pressure, electron pressure, experimental neutral pressure, experimental total pressure, and experimental electron pressure. The neutral pressure is decreased due to the pressure balance with plasma pressure (mainly electron pressure). A pressure probe was used to measure the total pressure with a thermal transpiration correction [17]. The neutral pressure was obtained from the measured total pressure and the electron pressure which is the product of the measured electron density and temperature profiles in fig. 1 (a) and (b).

Fig. 3 (c) shows the simulated neutral density, and experimental neutral density. The measured neutral density profile was obtained from the measured neutral temperature and neutral pressure with the assumption of ideal gas law ($p \sim nT$).

The excellent agreement between experiment and simulation was obtained for all neutral temperature, neutral pressure, and neutral density profiles.

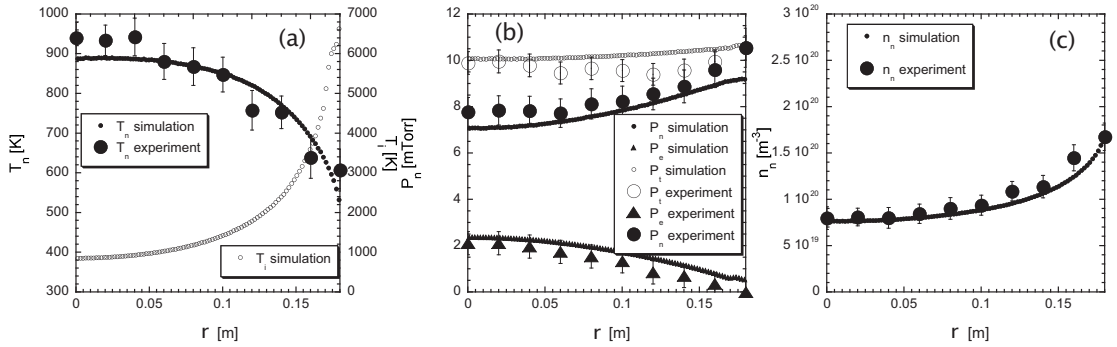

FIGURE 3. Comparison of Numerical and experimental results (a): Neutral temperature profile: the rotational temperature from second positive band of Nitrogen molecule (v',v")=(0,2) at 380 nm (large solid circles). Simulation neutral temperature (small solid circles) and simulation ion temperature (small open circles) (b): Neutral pressure profile: Simulation neutral pressure (small solid circles), simulation total pressure (small open circles) and simulation electron pressure (small open triagles). Experimental neutral pressure (large solid circles), experimental total pressure (large open circles) and experimental electron pressure (large open triagles). (c): Neutral density profile: Simulation neutral density (small solid circles), and experimental neutral density (large solid circles) All are in the condition $Ar/5\%N_2$ mixture. $p_{fill} = 10[\mathrm{mTorr}]$ and $P_{RF} = 2000\mathrm{W}$.

CONCLUSION

A hybrid type direct simulation Monte Carlo (DSMC) method for a one-dimensional (1D) electrostatic plasma was developed to understand the leading mechanism of the neutral gas depletion. The impact of the neutral depletion and the coupling between plasma and neutral gas were studied in weakly ionized unmagnetized plasma. The excellent agreement between experiment and simulation reveals that gas heating and pressure balance are main mechanisms of gas depletion in an inductively coupled plasma. At the high density plasma, where the plasma pressure becomes comparable to the fill pressure, significant neutral depletion occurs not only by gas heating but also by pressure balance. The resulting gas depletion enhances the plasma transport to the surrounding wall, increases the particle loss, and decreases the plasma density.

This work was supported by U.S. Department of Energy under DOE Grant No. DE-FG03-95ER5401.

REFERENCES

1. T. Hori, M. D. Bowden, K. Uchino, K. Muraoka, and M. Maeda, *J. Vac. Sci. Technol. A* **14**, 144 (1996).
2. P. W. Lee, and H. Y. Chang, *Phys. Lett. A* **213**, 186 (1996).
3. G. R. Tynan, and et al, *J. Vac. Sci. Technol. A* **15**, 2885 (1997).
4. G. R. Tynan, *J. Appl. Phys.* **86**, 5356 (1999).
5. S. Yun, K. Taylor, and G. R. Tynan, *Phys. Plasmas* **7**, 3448 (2000).
6. A. Fruchtman, and G. Makrinich, *Phys. Rev. Lett.* **95**, 115002 (2005).
7. G. A. Bird, Molecular Gas Dynamics and the Direct Simulation of Gas Flows *(Clarendon, Oxford)*, 1994.
8. V. V. Serikov, and K. Nanbu, *J. Appl. Phys.* **82**, 5948 (1997).
9. K. Nanbu, *IEEE trans. on Plasma Sci.* **28**, 971 (2000).
10. H. Akatsuka, A. N. Ezoubtshenko, and M. Suzuki, *J. Phys. D* **33**, 948 (2000).
11. M. A. Lieberman, and A. J. Lichtenburg, Principles of Plasma Discharges and Materials Processing *(New York, New York) Wiley-Interscience*, 1994.
12. P. C. Stangeby, The Plasma Boundary of Magnetic Fusion Devices *(Pristol, UK)*, *Inst. of Phys. Publishing*, 2000.
13. K.-U. Riemann, *J. Phys. D* **24**, 493 (1990).
14. K.-U. Riemann, *Phys. Plasmas* **4**, 4158 (1997).
15. J. F. O'Hanlon, A User's Guide to Vacuum Technology *(New York, New York) Wiley-Interscience*, 1989.
16. M. Shimada, G. R. Tynan, and R. Cattolica, *J. Vac. Sci. Technol. A accepted* (2006).
17. M. Shimada, G. R. Tynan, and R. Cattolica, *Plasma Source Sci. Technol. submitted* (2006).
18. E. C. Zipf, and R. W. McLaughlin, *Planet. Space Sci.* **26**, 449 (1978).
19. V. Guerra, and J. Loureiro, *Plasma Sources Sci. Technol.* **6**, 373 (1997).